

Ramsey spectroscopy, matter-wave interferometry, and the microwave-lensing frequency shift

Kurt Gibble

Department of Physics, The Pennsylvania State University, University Park, Pennsylvania 16802, USA

(Received 9 May 2014; published 14 July 2014; corrected 27 December 2017)

We derive the general frequency shift of a microwave atomic clock due to resonant dipole forces acting on the atomic wave functions during the Ramsey interactions. We explicitly demonstrate that only dressed-state populations in position space contribute significantly to the frequency shift and that the de Broglie phases of the dressed-state wave functions do not contribute. In addition, we show that momentum changes in the second Ramsey interaction normally produce negligible frequency shifts in comparison to those from the first Ramsey interaction.

DOI: [10.1103/PhysRevA.90.015601](https://doi.org/10.1103/PhysRevA.90.015601)

PACS number(s): 03.75.Dg, 06.30.Ft

Laser-cooled microwave atomic-fountain clocks currently provide the most accurate contributions to International Atomic Time (TAI) [1–5]. The accuracy of these standards continues to improve [1], with several clocks reporting accuracies of order 2×10^{-16} [2,4,5]. Significant recent advances have come from properly treating first-order Doppler shifts [2–8], reducing the uncertainty of frequency shifts from cold collisions [2,4,9,10], and theoretically evaluating the microwave-lensing frequency shift [2–5,11,12].

The scale of the microwave-lensing frequency shift is of order of the recoil shift [13] for a microwave photon, fractionally 1.5×10^{-16} [11,14]. Several clocks have corrected for this bias, using calculated shifts that range from 0.6×10^{-16} to 0.9×10^{-16} [2–4]. This shift is the largest bias applied to clocks that has not yet been experimentally observed. One group recently questioned the behavior and size of the microwave-lensing shift and reported a significantly smaller bias that they neglected [5,12]. To clarify the behavior of this shift, here we explicitly expand our previous treatment [11] and present a concise and intuitive calculation of this frequency shift, which agrees with [2–4,11].

Viewing a clock as a matter-wave interferometer [15] facilitates insight into the microwave lensing shift. In Fig. 1(a) an atom, localized to less than a wavelength of the oscillatory field, passes through the two separated interaction zones in Ramsey spectroscopy at t_1 and t_2 . The spatial variations of the dipole energy in the resonant microwave (or optical) standing waves deliver impulses to the dressed-state wave functions [11–18]. In a clock the temporal phase of the second Ramsey interaction at t_2 is shifted by $\chi = \pm\pi/2$ for the detected transition probability in Fig. 1(b) to be most sensitive to the phase of the coherent superposition of the two clock states [1]. The second interaction for $\chi = +(-)\pi/2$ transfers dressed state $|2(1)\rangle$ to the excited state [11], which is subsequently detected. Thus, because more of dressed state $|2\rangle$ passes through apertures in the clock, more excited-state atoms are detected for $\chi = +\pi/2$ than $-\pi/2$, producing a positive frequency shift of the clock's Ramsey fringe [11].

We begin with an interaction Hamiltonian $H_{\text{int}} = \hbar\omega\sigma_3/2 + \hbar\Omega(\vec{r},z)\cos(\omega t)\sigma_1$, which couples the ground and excited states of the clock transition, $|g\rangle$ and $|e\rangle$, in each Ramsey interaction in Fig. 1(a). Here ω is the resonant microwave frequency, Ω is the Rabi frequency, and σ are the Pauli matrices. Diagonalizing this Hamiltonian in the rotating-wave approximation leads to dressed states

$|1(2)\rangle = 2^{-1/2}(|g\rangle + (-)|e\rangle)$ and a Schrödinger equation $i\partial_t \psi(\vec{r},t)|\xi\rangle = (-\hbar\nabla^2/2m + \Omega(\vec{r},z)\sigma_3/2)\psi(\vec{r},t)|\xi\rangle$. The interactions with the standing-wave field are in the Raman-Nath regime [15], in which the kinetic energy during the interaction can be neglected, giving a unitary evolution of $\psi(\vec{r},t)|\xi\rangle$ [11]:

$$U(t^+,t^-) = \exp\left[-\frac{1}{2}i\phi(\vec{r})\sigma_3\right]. \quad (1)$$

Here the Rabi tipping angle $\phi(\vec{r})$ is $v_z^{-1} \int \Omega(\vec{r},z) dz$, the transverse position of the atoms is \vec{r} , and $\phi(\vec{r}) = \pi/2$ for spatially homogeneous $\pi/2$ pulses in the Ramsey interactions.

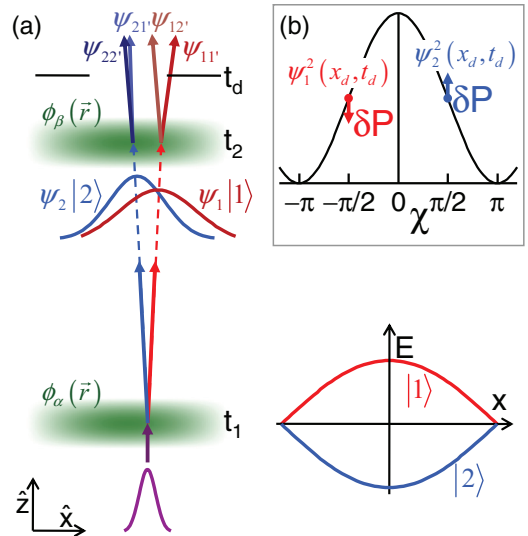


FIG. 1. (Color online) (a) The spatial gradients of the dipole energy in Ramsey spectroscopy deliver impulses to the atomic dressed-state wave functions, acting as positive lens for state $|2\rangle$ and negative lens for $|1\rangle$. The phase of the Ramsey field is shifted in the second interaction, giving dressed states $|1'\rangle$ and $|2'\rangle$, and four interferometer paths. The exaggerated deflections are of the order of nanometers, compared to centimeter widths of the atomic cloud. Apertures lead to a greater fraction of dressed state $|2\rangle$, $\psi_2(\vec{r},t_d)$ or equivalently $\psi_{21}(\vec{r},t_d)$ and $\psi_{22}(\vec{r},t_d)$, being detected than $|1\rangle$. (b) A clock's transition probability versus temporal phase χ of the second Ramsey interaction. The transition probability is most sensitive to χ at $\chi = \pm\pi/2$. For $\chi = +\pi/2$ the second Ramsey interaction transfers the incident dressed state $|2\rangle$ to the excited state and, for $\chi = -\pi/2$, $|1\rangle$ to the excited state. Because more of $\psi_2(\vec{r},t_d)$ passes through an aperture than of $\psi_1(\vec{r},t_d)$, the microwave lensing of wave functions produces a frequency shift of clocks.

We omit the velocity spread in the z direction, since it is typically small, but we treat arbitrary tipping angles so it can be effortlessly reintroduced.

The spatial gradient of the magnetic dipole energy $\hbar\Omega(\vec{r},t)$ delivers impulses to the dressed-state wave functions, deflecting them with small velocity changes and acting as a weak lens, slightly focusing $|2\rangle$ and defocusing $|1\rangle$ in Fig. 1(a) [11,12,16–18]. After the first Ramsey interaction, the dressed states propagate freely [$\Omega(\vec{r},z) = 0$] to the second interaction. The temporal phase χ of the second microwave field is changed to produce a Ramsey fringe. This gives new eigenstates for the second Ramsey interaction, $|1'\rangle$ and $|2'\rangle$, with a rotation $\cos(\chi/2)\hat{1} - i\sin(\chi/2)\sigma_1$ of $|1\rangle$ and $|2\rangle$. The second interaction also produces a unitary evolution (1), including deflections and further lensing, resulting in four dressed states at the exit of the interferometer. After both pulses, the excited-state population $|\psi(\vec{r},t_d)\langle e|\xi\rangle|^2$ is detected, yielding a Ramsey fringe. Explicitly, the evolution from the launch of the atoms at $t = 0$ in $|g\rangle$, through Ramsey interactions at t_1 and t_2 , to detection of $|e\rangle$, is

$$\psi(\vec{r},t_d)|\xi\rangle = U_{\text{free}}(t_d, T + t_1) \exp\left[-\frac{i}{2}\phi_\beta(\vec{r})\sigma_3\right] \cdot [\cos(\chi/2)\hat{1} - i\sin(\chi/2)\sigma_1]$$

$$\begin{aligned} \psi(\vec{r},t_d)\langle f|\xi\rangle|_{\chi=\pm\pi/2} &= \frac{\sqrt{2}}{4} \left\{ \psi_{11'}(\vec{r},t_d) \exp\left\{-i\left[\Phi_{11'}(\vec{r},t_d) + \frac{1}{2}\phi_\alpha(\vec{r}_1) + \frac{1}{2}\phi_\beta(\vec{r}_2)\right]\right\} \right. \\ &\quad \pm (-1)^{j_{eg}} i \psi_{12'}(\vec{r},t_d) \exp\left\{-i\left[\Phi_{12'}(\vec{r},t_d) + \frac{1}{2}\phi_\alpha(\vec{r}_1) - \frac{1}{2}\phi_\beta(\vec{r}_2)\right]\right\} \\ &\quad \mp i \psi_{21'}(\vec{r},t_d) \exp\left\{-i\left[\Phi_{21'}(\vec{r},t_d) - \frac{1}{2}\phi_\alpha(\vec{r}_1) + \frac{1}{2}\phi_\beta(\vec{r}_2)\right]\right\} \\ &\quad \left. - (-1)^{j_{eg}} \psi_{22'}(\vec{r},t_d) \exp\left\{-i\left[\Phi_{22'}(\vec{r},t_d) - \frac{1}{2}\phi_\alpha(\vec{r}_1) - \frac{1}{2}\phi_\beta(\vec{r}_2)\right]\right\} \right\}. \end{aligned} \quad (3)$$

Here $j_{eg} = 0$ if $\psi(\vec{r},t_d)|\xi\rangle$ is projected onto the excited state $\langle f| = |e\rangle$, and $j_{eg} = 1$ for detecting $\langle g|$. Since $|1'\rangle$ and $|2'\rangle$ in the second Ramsey interaction for $\chi = \pm\pi/2$ are equal superpositions of $|1\rangle$ and $|2\rangle$, there are four equally populated dressed states, with all combinations of focusing and defocusing after the two Ramsey interactions in Fig. 1(a). For example, $\psi_{21'}(\vec{r},t_d)\exp[-i\Phi_{21'}(\vec{r},t_d)]$ in (3) is focused in the first interaction and defocused in the second, and similarly for the other $\psi_{n,m}(\vec{r},t_d)\exp[-i\Phi_{n,m}(\vec{r},t_d)]$. For the perturbation expansion below, we have written the complex wave functions as real spatially dependent amplitudes $\psi_{n,m}(\vec{r},t_d)$ with complex phase factors $\exp[-i\Phi_{n,m}(\vec{r},t_d)]$. Further, we write each $\Phi_{n,m}(\vec{r},t_d)$ as $\Phi(\vec{r},t_d) + \delta\Phi_{n,m}(\vec{r})$, where a trivial common phase $\Phi(\vec{r},t_d)$ describes the propagation of the wave function for no Ramsey interactions and $\delta\Phi_{n,m}(\vec{r})$ is the change of the spatial phase due to the small dipole forces from the Ramsey interactions. In (3) we explicitly include the phase shifts $\phi_{\alpha,\beta}(\vec{r})$ of the dressed-state wave functions from the Ramsey interactions. Thus, the small dipole forces change the transition probability by δP [19], which gives the clock's

$$\begin{aligned} &\cdot U_{\text{free}}(T + t_1, t_1) \exp\left[-\frac{i}{2}\phi_\alpha(\vec{r})\sigma_3\right] \\ &\cdot U_{\text{free}}(t_1, 0) \psi(\vec{r}, 0) \frac{1}{\sqrt{2}} \begin{pmatrix} 1 \\ 1 \end{pmatrix}. \end{aligned} \quad (2)$$

Here we have allowed for different pulse areas $\phi_{\alpha,\beta}(\vec{r})$ and different spatial dependences in the two Ramsey interactions. If the Ramsey pulses $\phi_{\alpha,\beta}(\vec{r})$ are spatially homogeneous over the wave function, the free propagators are the same for all dressed states, and the same as for no Ramsey pulses, $\phi_{\alpha,\beta}(\vec{r}) = 0$. Thus, $\psi(\vec{r},t_d)\langle e|\xi\rangle = \{-i\sin[\phi_\alpha(\vec{r})/2 + \phi_\beta(\vec{r})/2]\cos(\chi/2) + \sin[\phi_\alpha(\vec{r})/2 - \phi_\beta(\vec{r})/2]\sin(\chi/2)\}\psi(\vec{r},t_d)$, which yields the expected Ramsey fringe versus the temporal phase χ .

We now calculate the general frequency shift of a clock due to the lensing of the atomic wave functions by the microwave standing waves. An atomic clock adjusts the oscillator's frequency so that the normalized transition probabilities on both sides of the central Ramsey fringe are equal. From (2), we calculate $\psi(\vec{r},t_d)\langle e|\xi\rangle|_{\chi=\pm\pi/2}$, including the lensing from the dipole impulses during the Ramsey interactions:

frequency shift:

$$\begin{aligned} \delta P &= \frac{1}{2} |\psi(\vec{r},t_d)\langle f|\xi\rangle|_{\chi=\pi/2}|^2 - \frac{1}{2} |\psi(\vec{r},t_d)\langle f|\xi\rangle|_{\chi=-\pi/2}|^2 \\ &= \frac{1}{4} (-1)^{j_{eg}} \{ \psi_{21'}(\vec{r},t_d)\psi_{22'}(\vec{r},t_d) \sin[\phi_\beta(\vec{r}_2) + \delta\Phi_{21'}(\vec{r}) \\ &\quad - \delta\Phi_{22'}(\vec{r})] - \psi_{11'}(\vec{r},t_d)\psi_{12'}(\vec{r},t_d) \sin[\phi_\beta(\vec{r}_2) \\ &\quad + \delta\Phi_{11'}(\vec{r}) - \delta\Phi_{12'}(\vec{r})] \} + \frac{1}{4} \{ \psi_{11'}(\vec{r},t_d)\psi_{21'}(\vec{r},t_d) \\ &\quad \times \sin[\phi_\alpha(\vec{r}_1) + \delta\Phi_{11'}(\vec{r}) - \delta\Phi_{21'}(\vec{r})] \\ &\quad - \psi_{12'}(\vec{r},t_d)\psi_{22'}(\vec{r},t_d) \sin[\phi_\alpha(\vec{r}_1) \\ &\quad + \delta\Phi_{12'}(\vec{r}) - \delta\Phi_{22'}(\vec{r})] \}. \end{aligned} \quad (4)$$

A key point that facilitates understanding the microwave-lensing frequency shift is that the small and somewhat complicated phase perturbations $\delta\Phi_{n,m}(\vec{r})$ do not contribute in lowest order. This leads to physical insight and dramatically

simplified our treatment in [11] and here, in contrast to the expressions in [12,14].

A quadratic spatial variation of the dipole energy and $\phi_{\alpha,\beta}(\vec{r})$ over the wave function $\psi_{n,m}(\vec{r},t_d)$ gives a Schrödinger propagation of a Gaussian wave function that reproduces a semiclassical view of dipole forces acting on the wave function [11]:

$$\psi_{x,21}(x,t_d) = \frac{e^{-\frac{1}{2}\left(\frac{x-x_d+\varepsilon_{\alpha x}(\vec{r}_1)-\varepsilon_{\beta x}(\vec{r}_2)-\varepsilon_{\alpha\beta x}}{w_{dx}-\delta_{\alpha x}+\delta_{\beta x}+\dots}\right)^2}}{\pi^{1/4}\sqrt{w_{dx}-\delta_{\alpha x}+\delta_{\beta x}+\dots}}. \quad (5)$$

Here $\psi_{2,1}(\vec{r},t_d)$ equals $\psi_{x,2,1}(x,t_d)\psi_{y,2,1}(y,t_d)$ and similarly for the three other $\psi_{n,m}(\vec{r},t_d)$'s. In (5) $w_x(t) = (\hbar^2 t^2/2m^2 \Delta_x^2 + 2\Delta_x^2)^{1/2}$ is the width and x_d is the center of the wave function at the detection time t_d , unperturbed by Ramsey interactions, $w_{dx} = w_x(t_d)$, $\varepsilon_{\alpha}(\vec{r}_1) = -\hbar(T+\Delta t_d)\nabla\phi_{\alpha}(\vec{r}_1)/2m$, and $\varepsilon_{\beta}(\vec{r}_2) = -\hbar\Delta t_d\nabla\phi_{\beta}(\vec{r}_2)/2m$ are the classical deflections of a particle traversing the Ramsey interactions at distances r_1 and r_2 off axis, and $\delta_{\alpha x} = -\hbar(T+\Delta t_d)w_x(t_1)\partial_x^2\phi_{\alpha}(x_1)/2m$ and $\delta_{\beta x} = -\hbar\Delta t_d w_x(t_2)\partial_x^2\phi_{\beta}(x_2)/2m$ give the focusing of the wave function. The deflection $\varepsilon_{\alpha,\beta}(\vec{r}_{1,2})$ and focusing $\delta_{\alpha,\beta}$ for a quadratic phase variation $\phi_{\alpha}(x) = \phi_{\alpha}(0)(1 - k_{\alpha x}^2 x^2/2)$ are proportional to the usual photon-recoil frequency shift $\nu_R = \hbar k_{\alpha x}^2/4\pi m$, which gives the scale of a clock's microwave-lensing frequency shift [11]. For cesium atoms at 1 μ K, the minimum wave function size $\Delta_{x,y}$ must be at least 30 nm and should be less than the 852 nm wavelength of the laser-cooling light [20,21], and $\varepsilon_{\alpha x}$ and $\delta_{\alpha x}$ are of order 4 and 2 nm [11], much less than w_{dx} in a clock, which is of order 1 cm. We can neglect the second-order deflection in the second Ramsey interaction due to the deflection $\varepsilon_{\alpha x}$ in the first, $\varepsilon_{\alpha\beta x} = \varepsilon_{\beta x}[\varepsilon_{\alpha x}(x_1)/(1+\Delta t_d/T)]$. The negligible ellipses in the denominators similarly represent changes in the wave function spreading due to the lensing and are, as a fraction of $\delta_{\alpha x}$, of order $\phi_{\beta}(0)\hbar\Delta t_d k_{\beta x}^2/m$, $\phi_{\alpha}(0)k_{\alpha x}^2\Delta^3/w_x(t_1)$, and smaller. We note that the Raman-Nath approximation in (1) does not include negligible displacements and phase shifts of short Ramsey interactions [12].

During the $T \approx 0.5$ s interrogation time of the clock, the atomic population enters and exits the clock's microwave cavity through its apertures. An atomic wave function that is of order 30 μ m wide spreads negligibly over this time. Because $\phi_{\alpha,\beta}(\vec{r})$ varies slowly over 30 μ m, we can semiclassically treat the atom propagation, originating from a point source and having classical trajectories with deflections of $\pm\varepsilon_{\alpha,\beta}(\vec{r}_{1,2})$ from the Ramsey interactions [2]. Note that (1)–(4) exactly treat the propagation through two Ramsey interactions, followed by an aperture, as in Fig. 1(a). In clocks, there are additional apertures, particularly before the first Ramsey interaction, as well as inhomogeneous detection of atoms [2–4,11]. This semiclassical approximation, which neglects the atomic diffraction of the apertures, simplifies the calculations and yields valuable clarity [2,11].

The δP 's from the x and y variations simply add, $\delta P = \delta P_x + \delta P_y$ [11], so we can treat each dimension separately.

Expanding (4) and substituting (5) gives, to first order in ν_R

$$\begin{aligned} \delta P_x = & \frac{1}{2}\psi_{0x}^2(x,t_d)\left\{(-1)^{j_{eg}}\left\{\frac{\delta_{\alpha x}}{w_{dx}}\left[1-2\left(\frac{x-x_d}{w_{dx}}\right)^2\right]\right.\right. \\ & \left.\left.-2\varepsilon_{\alpha x}(\vec{r}_1)\frac{x-x_d}{w_{dx}^2}\right\}\sin[\phi_{\beta}(\vec{r}_2)]\right. \\ & \left.-(-1)^{j_{ge}}\left\{\frac{\delta_{\beta x}}{w_{dx}}\left[1-2\left(\frac{x-x_d}{w_{dx}}\right)^2\right]\right.\right. \\ & \left.\left.-2\varepsilon_{\beta x}(\vec{r}_2)\frac{x-x_d}{w_{dx}^2}\right\}\sin[\phi_{\alpha}(\vec{r}_1)]\right\}. \quad (6) \end{aligned}$$

Here we have added 1_{ge} in the second term, which is 0 for entering the first Ramsey interaction in $|g\rangle$ and 1 for entering in $|e\rangle$, and $\psi_{0x}(x,t_d)$ is (5) with neither deflections $\varepsilon_{\alpha,\beta x}$ nor $\delta_{\alpha,\beta x}$.

The small phase variations $\delta\Phi_{n,m}(\vec{r})$ do not contribute to δP in (6), or to its associated frequency shift. To first order, the $\delta\Phi_{n,m}(\vec{r})$'s in (4) almost entirely cancel, with δP proportional to $[\delta\Phi_{11}(\vec{r}) - \delta\Phi_{12}(\vec{r}) - \delta\Phi_{21}(\vec{r}) + \delta\Phi_{22}(\vec{r})]/4$. Corrections include $\phi_{\alpha}(0)\phi_{\beta}(0)\hbar k_{\alpha x}^2 k_{\beta x}^2 x_1 x_2 t_1 \Delta t_d/m t_d$, which is of order nanoradians ($\delta\nu/\nu \approx 10^{-19}$), $2\phi_{\alpha}(0)\phi_{\beta}(0)\hbar k_{\alpha x}^2 k_{\beta x}^2 \Delta_x^2 t_1 \Delta t_d^2(T+\Delta t_d)/m t_d^3$, and smaller. This dramatically simplifies the calculation, which thus can be straightforwardly verified by reproducing the spinor algebra of (2)–(4). Further, $\psi_{x,21}(\vec{r},t_d)\psi_{x,22}(\vec{r},t_d)$ is $\psi_{x,2}(\vec{r},t_d)^2$ to first order in ε_{β} and $\delta_{\beta x,y}$ and $\psi_{x,11}(\vec{r},t_d)\psi_{x,12}(\vec{r},t_d)$ becomes $\psi_{x,1}(\vec{r},t_d)^2$. Below we show that the second term in (6) is almost always negligible, so (6) can be written as (2) in [11]:

$$\begin{aligned} \delta P_x = & \frac{1}{2}(-1)^{j_{eg}}[\psi_2^2(\vec{r},t_d) - \psi_1^2(\vec{r},t_d)]\sin[\phi_{\beta}(\vec{r}_2)] \\ = & \frac{(-1)^{j_{eg}}}{2}\psi_{0x}^2(x,t_d)\left\{\frac{\delta_{\alpha x}}{w_{dx}}\left[1-2\left(\frac{x-x_d}{w_{dx}}\right)^2\right]\right. \\ & \left.-2\varepsilon_{\alpha x}(\vec{r}_1)\frac{x-x_d}{w_{dx}^2}\right\}\sin[\phi_{\beta}(\vec{r}_2)]. \quad (7) \end{aligned}$$

Equation (7) has been evaluated for several fountain clocks [2–4]. Figure 2 depicts the change in transition probability that results from preferentially detecting dressed state $|2\rangle$ when an aperture transmits the center of the atomic cloud. Note that δP in (6) and (7) reverses sign if the ground state is detected instead of the excited state, a “flop-in” versus a “flop-out,” which gives

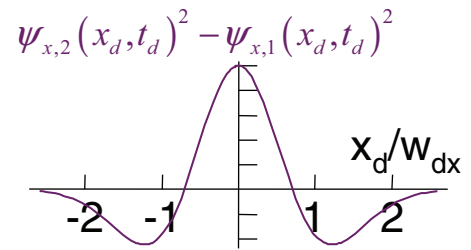


FIG. 2. (Color online) The spatial difference of dressed-state populations $|2\rangle$ and $|1\rangle$ of a centered cloud in the detection region. Apertures after the first Ramsey interaction transmit the center of the wave functions, leading to a frequency shift. Normally, the momentum changes in the second Ramsey interaction lead to small separations and do not produce a frequency shift.

the same frequency shift for both Ramsey fringes. However, if the initial state is the excited state instead of the ground state, the frequency shift reverses sign. Here, when detecting the excited state, δP is the same for entering the clock in either state but the Ramsey fringe has opposite signs for a flop-out versus a flop-in, reversing the frequency shift [11].

We get the frequency shift by integrating (7) over the spatial and velocity distributions, of widths w_{0x} and u , which are clipped by apertures of radii a_{1L} and a at t_{1L} and $t_{2L} \leq t_d$, before and after the Ramsey interactions [2–4]. Expressed as integrations over the circular apertures, δP is divided by the Ramsey fringe amplitude, and by $\pi(t_2 - t_1)$:

$$\begin{aligned} \frac{\delta \nu}{\nu_R} &= \frac{(-1)^{l_{se}} \phi_\alpha(0) \sin[\phi_\beta(0)] a(t_{2L} - t_1)}{\sin[\phi_\alpha(0)] \sin[\phi_\beta(0)] k(t_2 - t_1) \int_{r_{2L0} < a} \int_{r_{1L} < a_{1L}} \psi_0^2(\vec{r}_{2L0}, \vec{r}_{1L}) d\vec{r}_{1L} d\vec{r}_{2L0}} \\ &\times \int_0^{2\pi} \int_{r_{1L} < a_{1L}} \frac{r_{2L0}(t_1 - t_{1L}) + r_{1L}(t_{2L} - t_1) \cos(\phi_{2L0})}{|\vec{r}(t_1)| (t_{2L} - t_{1L})} J_1(k |\vec{r}(t_1)|) \psi_0^2(\vec{r}_{2L0}, \vec{r}_{1L}) \Big|_{r_{2L0}=a} d\vec{r}_{1L} d\phi_{2L0}, \\ \psi_0^2(\vec{r}_{2L0}, \vec{r}_{1L}) &= \exp \left[-\frac{r_{2L0}^2 w_{1L}^2 + r_{1L}^2 w_{2L}^2 - 2r_{2L0} r_{1L} (w_0^2 + u^2 t_{1L} t_{2L}) \cos(\phi_{2L0})}{w_0^2 u^2 (t_{2L} - t_{1L})^2} \right], \quad \vec{r}(t) = \frac{\vec{r}_{2L0}(t - t_{1L}) + \vec{r}_{1L}(t_{2L} - t)}{t_{2L} - t_{1L}}. \end{aligned} \quad (8)$$

Here we treat a cylindrical cavity, for which $\phi_{\alpha,\beta}(\vec{r}) = \phi_{\alpha,\beta}(0) J_0(kr)$ [2–4], $\cos(\phi_{2L0}) = \vec{r}_{2L0} \cdot \vec{r}_{1L}$, $u = (2k_B T/m)^{1/2}$ is the thermal velocity spread, w_0 is the initial e^{-1} cloud radius, and $w_{1L,2L}^2 = w_0^2 + u^2 t_{1L,2L}^2$. In (8) we have neglected the transverse variations of $\sin[\phi_\alpha(\vec{r})]$ and detection inhomogeneities, which were treated in [2–4] and normally give small corrections.

Note that the frequency shift (8) goes to a generally nonzero constant in the limit of zero amplitude of the microwave field, $\phi_\alpha(0) \rightarrow 0$. In this limit, the atoms have no dipole impulses so $\epsilon_\alpha(\vec{r}_1) \rightarrow 0$ and $\delta P \rightarrow 0$. However, the Ramsey fringe amplitude, the denominator in (8), is proportional to $\sin[\phi_\alpha(\vec{r})] \sin[\phi_\beta(\vec{r})]$ and also goes to 0. This is in contrast to [5,12], which consider that this frequency shift goes to 0 as $\phi_\alpha(0) = \phi_\beta(0) \rightarrow 0$.

Returning to the second term of (6), it is doubly small for $1, 3, 5, \dots, \pi/2$ Ramsey pulse areas. First, the time between the second interaction and detection $\Delta t_d = t_d - T - t_1$ (or an aperture at t_{2L}) is normally short compared to $T + \Delta t_d$. This gives little time for $\epsilon_{\beta x}$ and $\delta_{\beta x}$ to grow, as compared to $\epsilon_{\alpha x}$ and δ_α . If the detection is reasonably homogeneous, the effective aperture is the lower aperture of the cavity at time t_{2L} . This aperture typically produces a δP from the second term that is ≈ 10 times smaller than the first term. If the detection is inhomogeneous and near, or below, the launch region, the scale of the second term can be larger. However, second, this term gives the same δP when detecting the ground and excited states with the same homogeneity. As a fraction of the number of atoms that make it through the apertures in the clock, the number of excited-state atoms detected for $\chi = \pm\pi/2$ is $N_4 = \{1 - \cos[\phi_\alpha(\vec{r})] \cos[\phi_\beta(\vec{r})]\}/2 \pm \delta P_\alpha \sin[\phi_\beta(\vec{r})] \mp \delta P_\beta \sin[\phi_\alpha(\vec{r})]$ and the ground-state fraction ($j_{eg} = 1$) is $N_3 = \{1 + \cos[\phi_\alpha(\vec{r})] \cos[\phi_\beta(\vec{r})]\}/2 \mp \delta P_\alpha \sin[\phi_\beta(\vec{r})] \mp \delta P_\beta \sin[\phi_\alpha(\vec{r})]$. Thus, the normalized transition probability $N_4/N_3 + N_4$ usually has small changes. With the same approximations as in (8), the frequency shift is

$$\begin{aligned} \frac{\delta \nu}{\nu_R} &= -\cos[\phi_\alpha(0)] \cos[\phi_\beta(0)] \frac{(-1)^{l_{se}} \phi_\beta(0) \sin[\phi_\alpha(0)] a(t_{2L} - t_2)}{\sin[\phi_\alpha(0)] \sin[\phi_\beta(0)] k(t_2 - t_1) \int_{r_{2L0} < a} \int_{r_{1L} < a_{1L}} \psi_0^2(\vec{r}_{2L0}, \vec{r}_{1L}) d\vec{r}_{1L} d\vec{r}_{2L0}} \\ &\times \int_0^{2\pi} \int_{r_{1L} < a_{1L}} \frac{r_{2L0}(t_2 - t_{1L}) + r_{1L}(t_{2L} - t_2) \cos(\phi_{2L0})}{|\vec{r}(t_2)| (t_{2L} - t_{1L})} J_1(k |\vec{r}(t_2)|) \psi_0^2(\vec{r}_{2L0}, \vec{r}_{1L}) \Big|_{r_{2L0}=a} d\vec{r}_{1L} d\phi_{2L0}, \end{aligned} \quad (9)$$

where $\cos(\phi_{2L0}) = \hat{r}_{2L0} \cdot \hat{r}_{1L}$. Increasing the second pulse area $\phi_\beta(\vec{r})$ gives a larger frequency shift, until the average over the cosines suppresses the shift. However, note that (9) behaves differently from (8) since this frequency shift does not change sign as the atoms entering the clock are switched from $|g\rangle$ to $|e\rangle$. Thus, it will be difficult to experimentally observe (9) unless the large power dependence of distributed cavity phase shifts is highly suppressed [7,8].

In summary, the frequency shift due to the dipole forces on localized atoms from the exciting field depends to lowest order on only the populations of the four dressed-state wave functions that emerge from two Ramsey interactions. The phases from the small momentum changes that are imprinted

on dressed-state wave functions do not contribute, facilitating a simple physical picture of the shift: dressed state $|2\rangle$ is focused by the first Ramsey interaction and $|1\rangle$ is defocused. Therefore, apertures in the clock lead to a preferential detection of dressed state $|2\rangle$ and a frequency shift results [11]. We explicitly show that the momentum changes from the second Ramsey interaction zone produce naturally smaller perturbations that are further suppressed by reasonably similar or uniform state detection. While the microwave-lensing frequency shift has to be evaluated in the best clocks that currently contribute to atomic time, it has not yet been experimentally observed. Precise frequency measurements, while switching the initial state of the atoms between the ground and excited states with an increased

field strength during the first Ramsey interaction, $\phi_\alpha(\vec{r}) \approx 5\pi/2$, could reveal this frequency shift experimentally.

Note added in proof. Reference [22] also recently treated the microwave-lensing shift as 0 in the limit of zero microwave amplitude, in contrast to (8).

We gratefully acknowledge financial support from NASA and the NSF. I am grateful to S. R. Jeffers, T. P. Heavner, S. E. Barlow, and N. Ashby for bringing the typesetting errors to my attention.

-
- [1] R. Wynands and S. Weyers, *Metrologia* **42**, S64 (2005).
 - [2] R. Li, K. Gibble, and K. Szymaniec, *Metrologia* **48**, 283 (2011).
 - [3] S. Weyers, V. Gerginov, N. Nemitz, R. Li, and K. Gibble, *Metrologia* **49**, 82 (2011).
 - [4] J. Guéna, M. Abgrall, D. Rovera, Ph. Laurent, B. Chupin, M. Lours, G. Santarelli, P. Rosenbusch, M. E. Tobar, R. Li, K. Gibble, A. Clairon, and S. Bize, *IEEE Trans. Ultrason. Ferroelectr. Freq. Control* **59**, 391 (2012).
 - [5] T. P. Heavner, E. A. Donley, F. Levi, G. Costanzo, T. E. Parker, J. H. Shirley, N. Ashby, S. Barlow, and S. R. Jefferts, *Metrologia* **51**, 174 (2014).
 - [6] R. Li and K. Gibble, *Metrologia* **41**, 376 (2004).
 - [7] R. Li and K. Gibble, *Metrologia* **47**, 534 (2010).
 - [8] J. Guéna, R. Li, K. Gibble, S. Bize, and A. Clairon, *Phys. Rev. Lett.* **106**, 130801 (2011).
 - [9] K. Szymaniec, W. Chałupczak, E. Tiesinga, C. J. Williams, S. Weyers, and R. Wynands, *Phys. Rev. Lett.* **98**, 153002 (2007).
 - [10] F. Pereira Dos Santos, H. Marion, S. Bize, Y. Sortais, A. Clairon, and C. Salomon, *Phys. Rev. Lett.* **89**, 233004 (2002).
 - [11] K. Gibble, *Phys. Rev. Lett.* **97**, 073002 (2006).
 - [12] N. Ashby, S. Barlow, T. Heavner, and S. Jefferts, [arXiv:1404.4101v2](https://arxiv.org/abs/1404.4101v2).
 - [13] J. L. Hall, C. J. Bordé, and K. Uehara, *Phys. Rev. Lett.* **37**, 1339 (1976).
 - [14] P. Wolf and Ch. Borde, [arXiv:quant-ph/0403194](https://arxiv.org/abs/quant-ph/0403194). This work used a momentum basis which makes it difficult to accurately treat apertures in clocks, as well as momentum changes in two dimensions.
 - [15] A. D. Cronin, J. Schmiedmayer, and D. E. Pritchard, *Rev. Mod. Phys.* **81**, 1051 (2009).
 - [16] M. Bloom and K. Erdman, *Can. J. Phys.* **40**, 179 (1962).
 - [17] M. Bloom, E. Enga, and H. Lew, *Can. J. Phys.* **45**, 1481 (1967).
 - [18] T. Sleator, T. Pfau, V. Balykin, O. Carnal, and J. Mlynek, *Phys. Rev. Lett.* **68**, 1996 (1992).
 - [19] Note that δP here is half of δP in [11], consistent with [2–4,6–8].
 - [20] B. Saubaméa, T. W. Hijmans, S. Kulin, E. Rasel, E. Peik, M. Leduc, and C. Cohen-Tannoudji, *Phys. Rev. Lett.* **79**, 3146 (1997).
 - [21] P. D. Featonby, G. S. Summy, C. L. Webb, R. M. Godun, M. K. Oberthaler, A. C. Wilson, C. J. Foot, and K. Burnett, *Phys. Rev. Lett.* **81**, 495 (1998).
 - [22] F. Levi, D. Calonico, C. E. Calosso, A. Godone, S. Micalizio, and G. A. Costanzo, *Metrologia* **51**, 270 (2014).